

1

2 **Slope deformation, reservoir variation and meteorological data at the**
3 **Khoko landslide, Enguri hydroelectric basin (Georgia), during 2016-**
4 **2019**

5 Alessandro Tibaldi^{1*}, Federico Pasquaré Mariotto², Paolo Oppizzi³, Fabio Luca Bonali¹, Nino
6 Tsereteli⁴, Levan Mebonia⁵, Johni Chania⁵

7 ¹ Department of Earth and Environmental Sciences, University of Milan Bicocca, 20129 Milan, Italy

8 ² Department of Human and Innovation Sciences, Insubria University, Como, Italy

9 ³ Geolog.ch, Mendrisio, Switzerland

10 ⁴ Institute of Geophysics, University of Tbilisi, Tbilisi, Georgia

11 ⁵ Enguresi LtD Society, Georgia

12 *Corresponding Author: alessandro.tibaldi@unimib.it

13
14
15
16
17 **Abstract**
18 The Greater Caucasus mountain belt is characterized by deep valleys, steep slopes and frequent
19 seismic activity, the combination of which results in major landslide hazard. Along the eastern side
20 of the Enguri water reservoir lies the active Khoko landslide, whose head scarp zone affects the
21 important Jvari-Khaishi-Mestia road, one of the few connections with the interior of the Greater
22 Caucasus. Here, we present a database of measurement time series taken over a period of 4 years
23 (2016-2019) that enable to compare slope deformation with meteorological factors and man-induced
24 perturbations owing to variations in the water level of the reservoir. The monitoring system we used
25 is composed of two digital extensometers, placed within two artificial trenches excavated across the
26 landslide head scarp. The stations are equipped also with internal and near ground surface
27 thermometers. The data set is integrated by daily measurements of rainfall and lake level. The
28 monitoring system – the first installed in Georgia – was set up in the framework of a NATO-funded
29 project, aimed at assessing different types of geohazards affecting the Enguri artificial reservoir and
30 the related hydroelectrical plant. Our results indicate that the Khoko landslide displacements appear
31 to be mainly controlled by variations in hydraulic load, in turn induced by lake level oscillations.
32 Rainfall variations might also have contributed, though this is not always evident for all the studied
33 period. The full databases are freely available online at DOI: 10.20366/unimib/unidata/SI384-1.1
34 (Tibaldi et al., 2020).

35
36 **1 Introduction**
37 Landslides are widespread natural hazard sources, affecting most of the world's countries and capable
38 of causing serious economic losses. In fact, they can damage buildings, communication systems and

39 the overall environment. Moreover, these natural events are major cause of loss of life (Froude and
40 Petley, 2018). The monitoring of landslides is a necessary step to implement protective measures, as
41 it allows to recognize possible acceleration in slope deformation rate, alert residents or close road
42 communication systems, where needed. This type of monitoring is also of paramount importance for
43 assessing possible triggering factors (Casagli et al., 2009), determining the level of risk (Spiker and
44 Gori, 2003), and planning land use and risk management (Fell et al., 2005; Bertolini et al., 2005).
45 This activity can be of special relevance in case of complex situations, such as those affecting an
46 artificial water reservoir, where water variations can destabilize (or stabilize) the slopes overlooking
47 the basin. In such case, multiparameter data can be crosscut in order to look into possible correlations
48 between lake level variations, meteorological conditions, and slope deformations, which in turn are
49 key to effectively managing the filling and emptying of the reservoir.

50 The database of slope deformation can be derived from a variety of possible monitoring tools, which
51 range from on-site instruments to remotely controlled ones. The formers include continuous or
52 intermittent data collection, such as settlement gauges, inclinometers and piezometric groundwater
53 measurements (Liu and Wang, 2008). Surveys can be carried out by detecting surface movements of
54 unstable areas through levels, theodolites, Electronic Distance Measurement, and total station GPS
55 measurements (Liu Shao-tang, 2006). Remote control systems include aerial or terrestrial
56 photogrammetry in the visible or radar ranges (Bitelli et al., 2004). Monitoring the distance between
57 two points across the main landslide head scarp is the most effective way to describe the
58 displacements within the landslide, at a site far away from its toe. This is particularly helpful in
59 assessing the susceptibility of the whole landslide body to variations in toe conditions: in fact, a
60 feedback at the head scarp helps to decipher the long range of these effects.

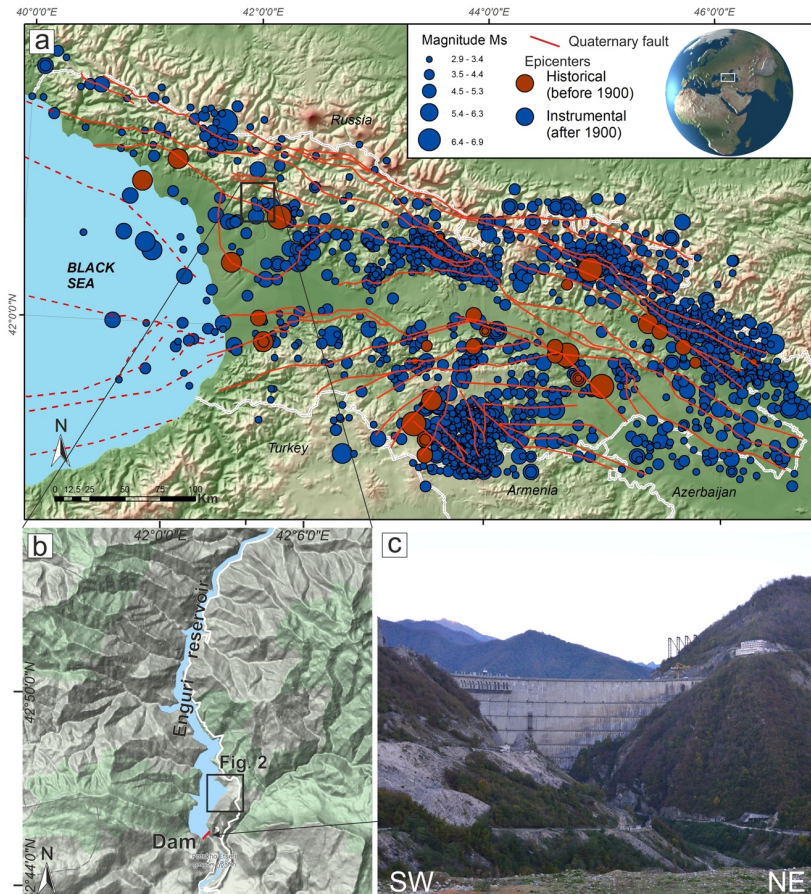
61 In November 2016, an international team of scientists, under the aegis of NATO, set about working
62 in the area of the Enguri artificial water reservoir, on the southwestern foothills of the Greater
63 Caucasus, Georgia (Fig. 1). During the first of several research missions, the team installed, for the
64 first time in Georgia, two digital extensometers across the head scarp of the major, active Khoko
65 landslide, located along the eastern mountain slope overlooking the reservoir. The associated
66 hydroelectrical plant, built during the Soviet era (Fig. 1c), is responsible for about half of the energy
67 supply to the country (Tibaldi et al. 2018). This monitoring activity is particularly relevant because
68 the study area is located in a region affected by widespread seismicity (Fig. 1a), associated with still
69 active mountain building processes, which have led to the formation of the Greater and Lesser
70 Caucasus, resulting from the continent–continent collision between the African–Arabian and
71 Eurasian plates (Reilinger 1997; 2006; Koçyigit et al. 2001; Pasquaré et al. 2011). Seismicity can
72 produce earthquake with Ms of 6-7 (Tsereteli et al., 2016) and macroseismic intensities up to 10

73 (Varazanashvili et al., 2018), as a consequence of active compressional tectonics (Tsereteli et al.,
74 2016; Tibaldi et al., 2017a, b, 2019). As broadly agreed upon in the scientific literature, there is a
75 tight connection between active tectonic processes and the occurrence of landslides (e.g. Tibaldi et
76 al. 2004, 2015; Tibaldi and Pasquaré, 2008; Pasquaré Mariotto and Tibaldi, 2016). As it is beyond
77 doubt that, in the future, a seismic event will happen again in the area, the installed monitoring
78 landslide system will be instrumental in quantitatively assessing the effects of ground shaking on
79 slope deformation rate.

80 Last but not least, the Jvari-Khaishi-Mestia road cuts across the uppermost portion of the Khoko
81 landslide, along a 2-km-long stretch, at an elevation of 700 m a.s.l. Several field surveys in the area
82 enabled the team to assess the presence of developing cracks, shear planes, opening of holes, and an
83 overall active deformation concentrated along 150-200-m-long road segments, which could pose
84 serious threats to road traffic security. These fractured zones are being continuously repaired by way
85 of asphalt refilling, with the purpose of preventing serious damage and road accidents.

86 We hereby provide and illustrate the database of measurements gathered by way of the integrated
87 monitoring system installed at the Khoko landslide. The main goals of our research are to identify
88 range and patterns of deformation, and assess possible relations between changes in water level at the
89 artificial Enguri reservoir, meteorological factors (temperature and rain) and slope deformations. The
90 analysis of these multi-temporal datasets is of broad interest, as it can provide a detailed framework
91 for planning the most appropriate actions in the management of major water reservoirs aimed at
92 energy production.

93



94

95 **Figure 1.** (a) Main historic and instrumental earthquake epicenters in the western Greater Caucasus; the
 96 black rectangle shows the area of Figure (b). White lines are country borders; the main Quaternary faults (red
 97 lines) are from Guler et al. (2011) and Tsereteli et al. (2016). Reference system: WGS84 / geographic coordinates. (b)
 98 DEM of the Enguri reservoir area, with dam location, © Google Maps. (c) Photo of the Enguri dam.

99

100 **2 Site description**

101 **2.1 Quaternary geology and geomorphology**

102 The study area is characterized by substrate rocks and widespread Quaternary deposits, which have
 103 been mapped thanks to a new geological survey, integrated with geological maps compiled prior to
 104 the creation of the artificial lake (Fig. 2). The studied slope is marked by landforms that are typical
 105 of recent/active gravitational deformation; the total surface area affected by slope instability, which

106 is about 1.2 km², is characterized by debris deposits, colluvium deposits, alluvial deposits, ancient
107 landslide deposits (Fig. 2) and fractured substrate rocks. Debris deposits are widespread in the lower
108 parts of the mountain located in the southern sector of the study area, outside the landslide area. They
109 can be observed also at the head scarp of the landslide. Colluvium deposits mantle the central part of
110 the landslide body and the lowermost slope in the southwestern sector of the study area. Landslide
111 deposits are widespread in the upper portion of the landslide body. Alluvial deposits are located along
112 the trace of the old Enguri river, now below the artificial lake's level.

113 At an altitude of 720-740 m, a number of scarps can be noticed, facing westward and affecting the
114 Jvari-Khaishi-Mestia road (Figs. 2 and 3). The height of such scarps ranges from 20 m to 70 m,
115 representing the head scarps. These scarps cannot be the effect of roadcut during the road construction
116 because these scarps are longer than the road, and thus the road only in part follows the scarp. In fact,
117 the scarp prolongs outward from the road in the northern part. Moreover, the road cuts through the
118 scarp in the southern part. Finally, the very large height of these scarps is poorly compatible with the
119 supposed cut of a small road, especially considering that this scarp height is present also outside of
120 the road. At the foot of the scarps, the topography is either horizontal or gently dipping westward,
121 suggesting a possible uphill tilting of the slope (Fig. 3a). The asphalted surface of the road here is
122 affected by fissures, as wide as a few centimeters, and by westward-facing, 20-cm-high (in 2016)
123 scarps (Fig. 3d). These structures are parallel to sub-parallel to the morphological high head scarps.
124 As documented by Tibaldi et al. (2019), in the forest across the southern segment of the head scarps,
125 tens of meters long, and up to 3.8 m wide fissures were found. Some of the trees, with trunks of about
126 20 cm in diameter, grew inside the fissures, suggesting that the fissures have a long history, at least
127 dating back to several tens of years (Tibaldi et al., 2019).

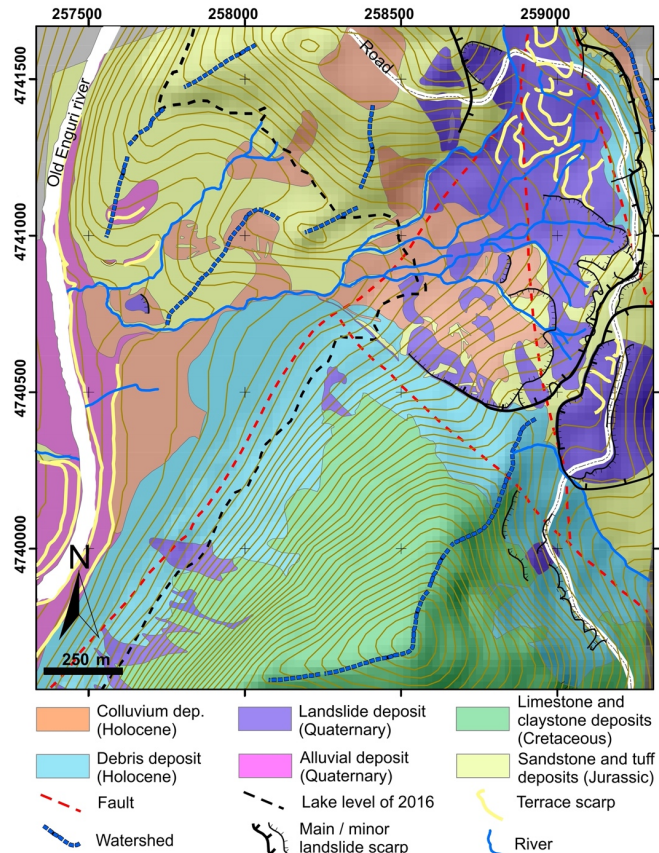
128 Downhill from the head scarp, several changes of inclination affect the slope, resulting in a series of
129 downhill-facing scarps. Most are oriented perpendicularly to the local slope dip and can be observed
130 in the upper part of the slope. This suggests the possible presence of secondary landslide slip planes
131 (Tibaldi et al., 2019). Besides, most of the studied slope is characterized by the presence of several
132 tilted trees; moreover, locally all of the trunks are tilted, and this is another indicator of active slope
133 deformation (Fig. 3c).

134 The arrangement of river streams, as shown Figure 2, is based on the present-day river network and
135 Soviet-era topographic maps compiled before the build-up of the water reservoir. In the slope section
136 above the present-day lake, the rivers mostly follow the average slope dip, according to a dendritic
137 pattern. Below the present-day lake level, one single stream was draining the landslide area. Here, at
138 the toe of the slope, this single stream was running parallel to the main Enguri river but with a
139 northward, opposite flow (Tibaldi et al., 2019). This is an anomaly in the stream pattern that can be

Eliminato: .

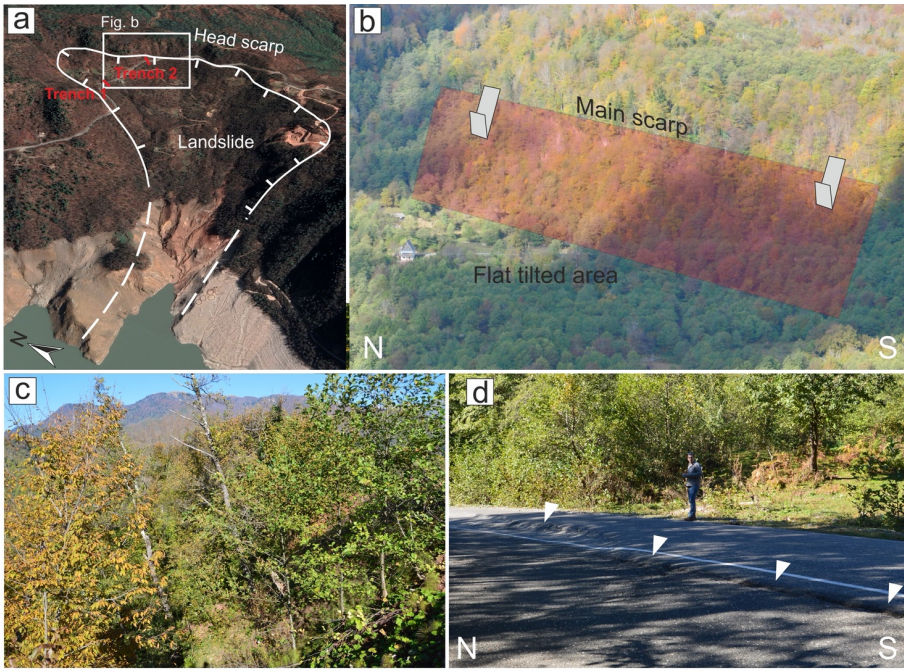
141 linked to a disturbance in the average slope topography, suggesting a possible early bulging of the
142 landslide toe.

143



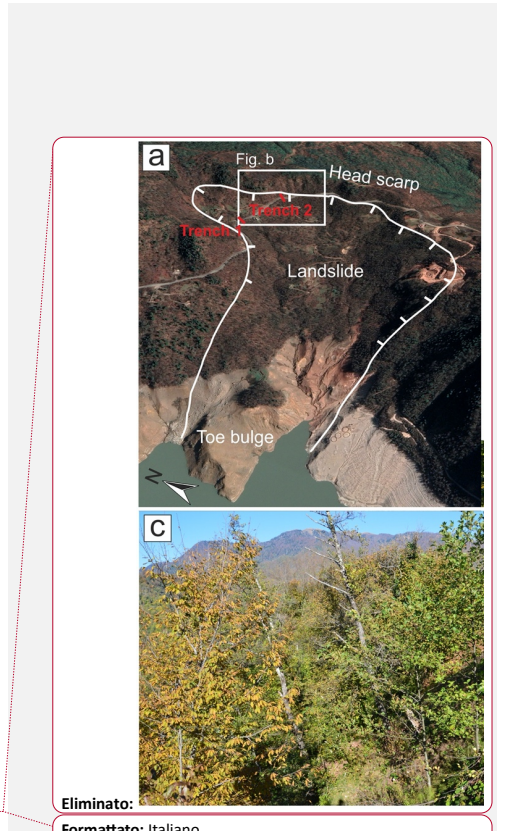
144
145 **Figure 2.** Geological and geomorphological map of the study area, modified after Tibaldi et al. (2019).
146 Location in Figure 1b.

147



148 **Figure 3.** (a) Oblique view of the studied landslide (© Google Earth); trench locations are shown.
149 (b) Photo of a segment of the landslide head scarp; it is worth noticing the flat-lying area at the foot
150 of the scarp, created by the uphill tilting of the slope during rotational movements of the landslide
151 block. House for scale (left hand side of the flat area). (c) Example of tilted trees along the landslide
152 slope. (d) Photo of the escarpments cutting the Jvari-Khaishi-Mestia road (white triangles),
153 representing the surface expression of active landslide slip planes.

154
155
156 **2.2 Substrate description**
157 Around the landslide area, Jurassic volcanic and terrigenous rocks and Cretaceous carbonate deposits
158 crop out (Fig. 2), generally dipping to the south. The inclination of the Cretaceous strata cropping out
159 around the Enguri dam is in the order of 60-70°, whereas the bedding attains a shallower dip
160 northward, becoming sub-horizontal toward the northern part of the reservoir. Below the carbonate
161 layers, Jurassic deposits can be observed, made of sandstones, tuffs, tuff-breccia and gypsum layers
162 that crop out locally along the southeastern slopes of the reservoir. In the landslide area, essentially
163 Jurassic and Quaternary deposits crop out. Here, most of the Jurassic rocks dip to the east, with slight
164 variations (Fig. 4b). Presently, gypsum is excavated from a small mine, for economic purposes. Near



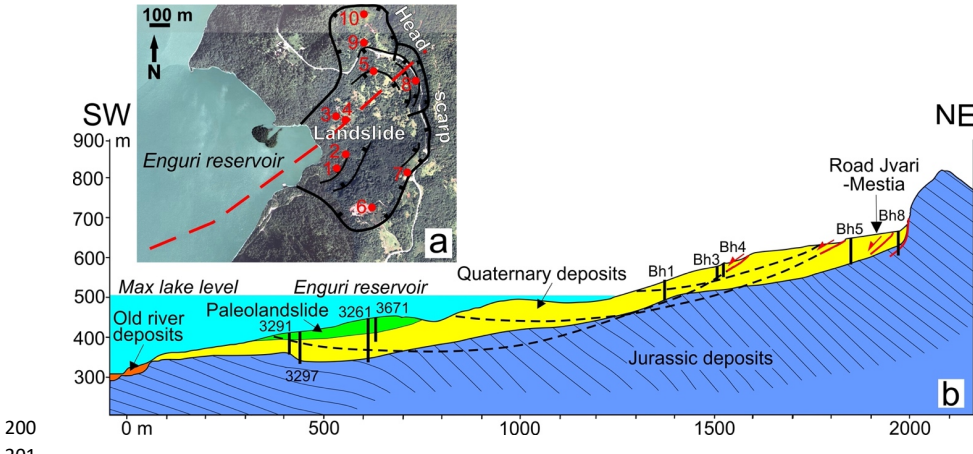
155
156
157
158
159
160
161
162
163
164
165
166
167
168
169
170
171
172
173
174
175
176
177
178
179
180
181
182
183
184
185
186
187
188
189
190
191
192
193
194
195
196
197
198
199
200
201
202
203
204
205
206
207
208
209
210
211
212
213
214
215
216
217
218
219
220
221
222
223
224
225
226
227
228
229
230
231
232
233
234
235
236
237
238
239
240
241
242
243
244
245
246
247
248
249
250
251
252
253
254
255
256
257
258
259
260
261
262
263
264
265
266
267
268
269
270
271
272
273
274
275
276
277
278
279
280
281
282
283
284
285
286
287
288
289
290
291
292
293
294
295
296
297
298
299
300
301
302
303
304
305
306
307
308
309
310
311
312
313
314
315
316
317
318
319
320
321
322
323
324
325
326
327
328
329
330
331
332
333
334
335
336
337
338
339
340
341
342
343
344
345
346
347
348
349
350
351
352
353
354
355
356
357
358
359
360
361
362
363
364
365
366
367
368
369
370
371
372
373
374
375
376
377
378
379
380
381
382
383
384
385
386
387
388
389
390
391
392
393
394
395
396
397
398
399
400
401
402
403
404
405
406
407
408
409
410
411
412
413
414
415
416
417
418
419
420
421
422
423
424
425
426
427
428
429
430
431
432
433
434
435
436
437
438
439
440
441
442
443
444
445
446
447
448
449
450
451
452
453
454
455
456
457
458
459
460
461
462
463
464
465
466
467
468
469
470
471
472
473
474
475
476
477
478
479
480
481
482
483
484
485
486
487
488
489
490
491
492
493
494
495
496
497
498
499
500
501
502
503
504
505
506
507
508
509
510
511
512
513
514
515
516
517
518
519
520
521
522
523
524
525
526
527
528
529
530
531
532
533
534
535
536
537
538
539
540
541
542
543
544
545
546
547
548
549
550
551
552
553
554
555
556
557
558
559
560
561
562
563
564
565
566
567
568
569
570
571
572
573
574
575
576
577
578
579
580
581
582
583
584
585
586
587
588
589
590
591
592
593
594
595
596
597
598
599
600
601
602
603
604
605
606
607
608
609
610
611
612
613
614
615
616
617
618
619
620
621
622
623
624
625
626
627
628
629
630
631
632
633
634
635
636
637
638
639
640
641
642
643
644
645
646
647
648
649
650
651
652
653
654
655
656
657
658
659
660
661
662
663
664
665
666
667
668
669
670
671
672
673
674
675
676
677
678
679
680
681
682
683
684
685
686
687
688
689
690
691
692
693
694
695
696
697
698
699
700
701
702
703
704
705
706
707
708
709
710
711
712
713
714
715
716
717
718
719
720
721
722
723
724
725
726
727
728
729
730
731
732
733
734
735
736
737
738
739
740
741
742
743
744
745
746
747
748
749
750
751
752
753
754
755
756
757
758
759
750
751
752
753
754
755
756
757
758
759
760
761
762
763
764
765
766
767
768
769
770
771
772
773
774
775
776
777
778
779
770
771
772
773
774
775
776
777
778
779
780
781
782
783
784
785
786
787
788
789
780
781
782
783
784
785
786
787
788
789
790
791
792
793
794
795
796
797
798
799
800
801
802
803
804
805
806
807
808
809
800
801
802
803
804
805
806
807
808
809
810
811
812
813
814
815
816
817
818
819
810
811
812
813
814
815
816
817
818
819
820
821
822
823
824
825
826
827
828
829
820
821
822
823
824
825
826
827
828
829
830
831
832
833
834
835
836
837
838
839
830
831
832
833
834
835
836
837
838
839
840
841
842
843
844
845
846
847
848
849
840
841
842
843
844
845
846
847
848
849
850
851
852
853
854
855
856
857
858
859
850
851
852
853
854
855
856
857
858
859
860
861
862
863
864
865
866
867
868
869
860
861
862
863
864
865
866
867
868
869
870
871
872
873
874
875
876
877
878
879
870
871
872
873
874
875
876
877
878
879
880
881
882
883
884
885
886
887
888
889
880
881
882
883
884
885
886
887
888
889
890
891
892
893
894
895
896
897
898
899
900
901
902
903
904
905
906
907
908
909
900
901
902
903
904
905
906
907
908
909
910
911
912
913
914
915
916
917
918
919
910
911
912
913
914
915
916
917
918
919
920
921
922
923
924
925
926
927
928
929
920
921
922
923
924
925
926
927
928
929
930
931
932
933
934
935
936
937
938
939
930
931
932
933
934
935
936
937
938
939
940
941
942
943
944
945
946
947
948
949
940
941
942
943
944
945
946
947
948
949
950
951
952
953
954
955
956
957
958
959
950
951
952
953
954
955
956
957
958
959
960
961
962
963
964
965
966
967
968
969
960
961
962
963
964
965
966
967
968
969
970
971
972
973
974
975
976
977
978
979
970
971
972
973
974
975
976
977
978
979
980
981
982
983
984
985
986
987
988
989
980
981
982
983
984
985
986
987
988
989
990
991
992
993
994
995
996
997
998
999
1000
1001
1002
1003
1004
1005
1006
1007
1008
1009
1000
1001
1002
1003
1004
1005
1006
1007
1008
1009
1010
1011
1012
1013
1014
1015
1016
1017
1018
1019
1010
1011
1012
1013
1014
1015
1016
1017
1018
1019
1020
1021
1022
1023
1024
1025
1026
1027
1028
1029
1020
1021
1022
1023
1024
1025
1026
1027
1028
1029
1030
1031
1032
1033
1034
1035
1036
1037
1038
1039
1030
1031
1032
1033
1034
1035
1036
1037
1038
1039
1040
1041
1042
1043
1044
1045
1046
1047
1048
1049
1040
1041
1042
1043
1044
1045
1046
1047
1048
1049
1050
1051
1052
1053
1054
1055
1056
1057
1058
1059
1050
1051
1052
1053
1054
1055
1056
1057
1058
1059
1060
1061
1062
1063
1064
1065
1066
1067
1068
1069
1060
1061
1062
1063
1064
1065
1066
1067
1068
1069
1070
1071
1072
1073
1074
1075
1076
1077
1078
1079
1070
1071
1072
1073
1074
1075
1076
1077
1078
1079
1080
1081
1082
1083
1084
1085
1086
1087
1088
1089
1080
1081
1082
1083
1084
1085
1086
1087
1088
1089
1090
1091
1092
1093
1094
1095
1096
1097
1098
1099
1090
1091
1092
1093
1094
1095
1096
1097
1098
1099
1100
1101
1102
1103
1104
1105
1106
1107
1108
1109
1100
1101
1102
1103
1104
1105
1106
1107
1108
1109
1110
1111
1112
1113
1114
1115
1116
1117
1118
1119
1110
1111
1112
1113
1114
1115
1116
1117
1118
1119
1120
1121
1122
1123
1124
1125
1126
1127
1128
1129
1120
1121
1122
1123
1124
1125
1126
1127
1128
1129
1130
1131
1132
1133
1134
1135
1136
1137
1138
1139
1130
1131
1132
1133
1134
1135
1136
1137
1138
1139
1140
1141
1142
1143
1144
1145
1146
1147
1148
1149
1140
1141
1142
1143
1144
1145
1146
1147
1148
1149
1150
1151
1152
1153
1154
1155
1156
1157
1158
1159
1150
1151
1152
1153
1154
1155
1156
1157
1158
1159
1160
1161
1162
1163
1164
1165
1166
1167
1168
1169
1160
1161
1162
1163
1164
1165
1166
1167
1168
1169
1170
1171
1172
1173
1174
1175
1176
1177
1178
1179
1170
1171
1172
1173
1174
1175
1176
1177
1178
1179
1180
1181
1182
1183
1184
1185
1186
1187
1188
1189
1180
1181
1182
1183
1184
1185
1186
1187
1188
1189
1190
1191
1192
1193
1194
1195
1196
1197
1198
1199
1190
1191
1192
1193
1194
1195
1196
1197
1198
1199
1200
1201
1202
1203
1204
1205
1206
1207
1208
1209
1200
1201
1202
1203
1204
1205
1206
1207
1208
1209
1210
1211
1212
1213
1214
1215
1216
1217
1218
1219
1210
1211
1212
1213
1214
1215
1216
1217
1218
1219
1220
1221
1222
1223
1224
1225
1226
1227
1228
1229
1220
1221
1222
1223
1224
1225
1226
1227
1228
1229
1230
1231
1232
1233
1234
1235
1236
1237
1238
1239
1230
1231
1232
1233
1234
1235
1236
1237
1238
1239
1240
1241
1242
1243
1244
1245
1246
1247
1248
1249
1240
1241
1242
1243
1244
1245
1246
1247
1248
1249
1250
1251
1252
1253
1254
1255
1256
1257
1258
1259
1250
1251
1252
1253
1254
1255
1256
1257
1258
1259
1260
1261
1262
1263
1264
1265
1266
1267
1268
1269
1260
1261
1262
1263
1264
1265
1266
1267
1268
1269
1270
1271
1272
1273
1274
1275
1276
1277
1278
1279
1270
1271
1272
1273
1274
1275
1276
1277
1278
1279
1280
1281
1282
1283
1284
1285
1286
1287
1288
1289
1280
1281
1282
1283
1284
1285
1286
1287
1288
1289
1290
1291
1292
1293
1294
1295
1296
1297
1298
1299
1290
1291
1292
1293
1294
1295
1296
1297
1298
1299
1300
1301
1302
1303
1304
1305
1306
1307
1308
1309
1300
1301
1302
1303
1304
1305
1306
1307
1308
1309
1310
1311
1312
1313
1314
1315
1316
1317
1318
1319
1310
1311
1312
1313
1314
1315
1316
1317
1318
1319
1320
1321
1322
1323
1324
1325
1326
1327
1328
1329
1320
1321
1322
1323
1324
1325
1326
1327
1328
1329
1330
1331
1332
1333
1334
1335
1336
1337
1338
1339
1330
1331
1332
1333
1334
1335
1336
1337
1338
1339
1340
1341
1342
1343
1344
1345
1346
1347
1348
1349
1340
1341
1342
1343
1344
1345
1346
1347
1348
1349
1350
1351
1352
1353
1354
1355
1356
1357
1358
1359
1350
1351
1352
1353
1354
1355
1356
1357
1358
1359
1360
1361
1362
1363
1364
1365
1366
1367
1368
1369
1360
1361
1362
1363
1364
1365
1366
1367
1368
1369
1370
1371
1372
1373
1374
1375
1376
1377
1378
1379
1370
1371
1372
1373
1374
1375
1376
1377
1378
1379
1380
1381
1382
1383
1384
1385
1386
1387
1388
1389
1380
1381
1382
1383
1384
1385
1386
1387
1388
1389
1390
1391
1392
1393
1394
1395
1396
1397
1398
1399
1390
1391
1392
1393
1394
1395
1396
1397
1398
1399
1400
1401
1402
1403
1404
1405
1406
1407
1408
1409
1400
1401
1402
1403
1404
1405
1406
1407
1408
1409
1410
1411
1412
1413
1414
1415
1416
1417
1418
1419
1410
1411
1412
1

166 the coast of the artificial lake, at the foot of the onshore section of the landslide, there are intensely
167 deformed gypsum rocks.

168 The complexity of the geometry of the head scarps as well as the morphology of the slope, and the
169 size of the whole unstable slope, suggest that the landslide slip surface is not unique and probably
170 there are different, partially superimposed slip planes. This interpretation is supported by the analysis
171 of the state of preservation of piezometers located in the landslide body. We checked the instruments
172 and noticed that most of the piezometers installed during 2015 across the landslide, are interrupted at
173 depths between 16 and 42 m (Table 1). Although the a priori hypothesis must be mentioned that these
174 interruptions may have been produced by infiltration of fine material into the piezometers, we made
175 the measurements in May 2017, only two years after their installation, thus the very recent age of the
176 piezometers suggests that these may be the depths where the piezometric logs are intersected by the
177 sliding surfaces of active landslides. This is supported by the observation that close piezometers,
178 originally excavated down to different depths, are now interrupted at the same depth, such as BH3
179 and BH4 cut at -16 m, and BH1 and BH2 cut at -35-36 m. The fact that in general these ruptures are
180 located at different depths indicates the presence of different slip planes.

181 Other logs were drilled during the Soviet era to reconstruct the rock distribution in the substrate. An
182 analysis of the lithological characteristics of the logs shows that the intact substrate rock is located at
183 deeper levels, in the order of several tens of meters. For example, logs 3261 and 3297 (drilled in
184 1966) (Fig. 4b) show the presence of clastic, unconsolidated deposits, rich in clay and locally gypsum
185 fragments, down to a depth of 57.5 m (log 3297), and/or clastic deposits with a sill to clay matrix
186 down to at least 61 m (log 3297) and at least 80 m (log 3261). Log 3291 (also drilled in 1966) shows
187 the presence of clay and gypsum deposits down to a depth of 30 m, and of the substrate at greater
188 depths. The geological survey integrated with the observations of the logs and piezometers enabled
189 us to prepare the geological section of Figure 4b, which extends across the onshore landslide portion
190 and below the lake (Fig. 4a). The section indicates that the intact substrate rock is always deeper than
191 30 m, down to 80 m. In this section, we added the head scarps of slip planes as observed in the field
192 (red lines), and the main slip surfaces (dashed black lines) as obtained by a numerical slope analysis
193 performed by Tibaldi et al. (2019). The analysis was carried out considering different levels of the
194 lake reservoir; in the section are represented: i) the deepest slip surface (corresponding to $FS < 1$)
195 among those obtained with a maximum of 510 m a.s.l. of the reservoir water level (this surface starts
196 at log BH4), ii) the deepest slip surface (corresponding to $FS < 1$) among those calculated with a
197 minimum of 430 m a.s.l. of the reservoir water level (this surface starts at log BH3), and iii) the
198 shallowest slip surface that is present in both scenarios of lake level.

199



202 **Figure 4.** (a) Trace (red dashed line) of the geological section and location (red dots) of the
 203 piezometers described in Table 1. Black lines are major landslide scarps. (b) Geological section
 204 across the slope facing the Enguri reservoir. Black columns represent locations and depth of logs
 205 used to construct the cross section. Dashed black lines are the main potential slip surfaces calculated
 206 through a static analysis by Tibaldi *et al.* (2019), red lines with arrows are landslide scarps surveyed
 207 in the field. Data of the submerged part are derived from geological surveys made in the Soviet era,
 208 before the construction of the dam.

209
 210 **Table 1.** Characteristics of measured piezometers and water table depth; b.g.s. refers to depths
 211 below ground surface.

Site	Easting (dd.ddd)	Northing (dd.ddd)	Elevation (m)	Installed total depth (m b.g.s.)	Measured depth to water (m b.g.s.)	Measured depth to bottom (m b.g.s.)
BH1	42.049950	42.781550	566.6	45	7,4	35
BH2	42.050650	42.782500	568.2	50	1,5	36
BH3	42.049850	42.784583	587	32	1,3	16
BH4	42.050583	42.784417	652,8	65	1,3	16
BH5	42.052633	42.787150	679,7	50	0,5	42
BH6	42.053017	42.779717	725,9	50	12,0	18
BH7	42.055433	42.781700	721,3	50	5,8	49
BH8	42.055883	42.786517	704	55	4,8	23
BH9	42.051800	42.788767	702,6	51	0,2	37
BH10	42.051800	42.790167	727,9	50	Broken	Broken

212

213 **3 Methodology and instrumentation**

214 In 2016, two trenches were excavated across the main head scarps of the Khoko landslide, separated
215 by about 240 m. The location of the sites selected for trenching is indicated in Figure 3a, and these
216 locations were based upon the presence of clear indicators of active deformation on the road, at the
217 foot of the main landslide scarps. Each of the two trenches was suitable for hosting a horizontal,
218 digital extensometer (Wire Linear Potentiometric Transducer, SF500). The two trenches were opened
219 perpendicularly to the scarp strike, crossing the road at a high angle (Fig. 5a). The instrumentation
220 was placed within a protection system aimed at avoiding disturbance or damage from heavy load
221 traffic (Figs. 5b-d). The opening of the trenches was performed in two stages, so as to enable vehicles
222 to drive through the area along alternating lanes. The protection of the measurement stations consists
223 of a channel in reinforced concrete, buried down to a depth of at least 50 cm.

224 The instrument is composed of a wire, a digital meter, and a recorder system. The stainless steel wire
225 changes its length based on the relative movements of the piercing points to which it is connected.
226 The wire was inserted into a pipe, laid down horizontally and protected with sand (Fig. 5c-d). At both
227 ends, steel pipes were positioned, aimed at securing the measurement wire and the electronic
228 instrumentation. Each vertical tube was equipped with a steel cover and gasket. The two covers were
229 buried underneath a 15 cm-thick soil layer. These operations were made more difficult by the presence
230 of a pavement in concrete beneath the present-day asphalt layer. The meter is a wire potentiometric
231 position transducer that turns a linear motion into a resistance variation. It is made of a precision
232 rotating potentiometer operated by the winding or unwinding stainless steel wire.

233 Due to the impossibility of transmitting the data directly to a computer at the Enguri dam premises or
234 via internet (due to the remoteness of the site), the measurements have been stored in a digital recorder
235 (data logger THEMIS-USB-GPRS) and downloaded on a 30-day basis. The system is connected to a
236 set of insulated batteries with a life of 6 months.

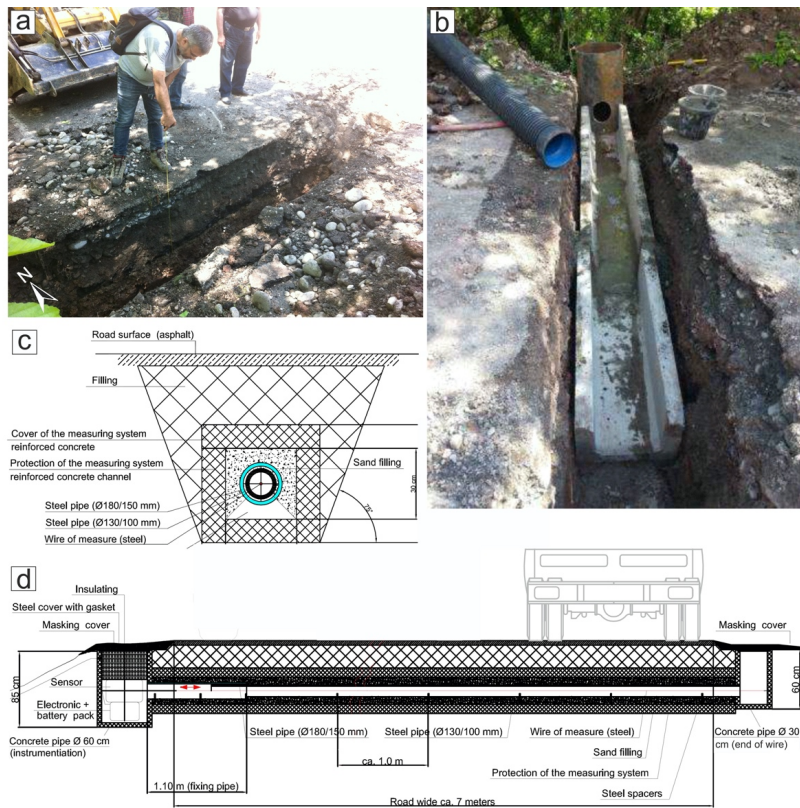
237 Extensometer n. 1 was put in operation in November 2016, whereas the second extensometer began
238 recording data in May 2017. The instruments include also an internal and external sensor of
239 temperature - PT100.

240 The station for measuring the Enguri lake level is installed at an altitude of 360 m in the dam. It is
241 made of a Multi-Channel Recorder RSG30 Ecograph T, by Endress+Hauser, using the Software
242 ETU00xA, V2.02.xx. The data are transmitted in real-time to the dam administration and stored in
243 local computers.

244 Rainfall amounts are recorded by a station, situated at an altitude of 540 m near the dam's
245 administrative building. The station features the Davis Vantage Pro2 instrument, suitable for

246 measuring rainfall, wind speed, temperature and humidity, with data updated every 2.5 seconds. It
 247 comes with a self-emptying tipping spoon determining rainfall amounts in 0.2 mm increments, and is
 248 laser-calibrated for increasing accuracy. The data are transmitted in real-time to the dam
 249 administration and stored in local computers.

250



251
 252 **Figure 5.** (a) Opening of trench n. 1. (b) Installation of the concrete protection for the extensometer.
 253 (c) Section transversal to the extensometer system. (d) Longitudinal section of the extensometer
 254 system. Location of the two measurement stations provided in Figure 3a.

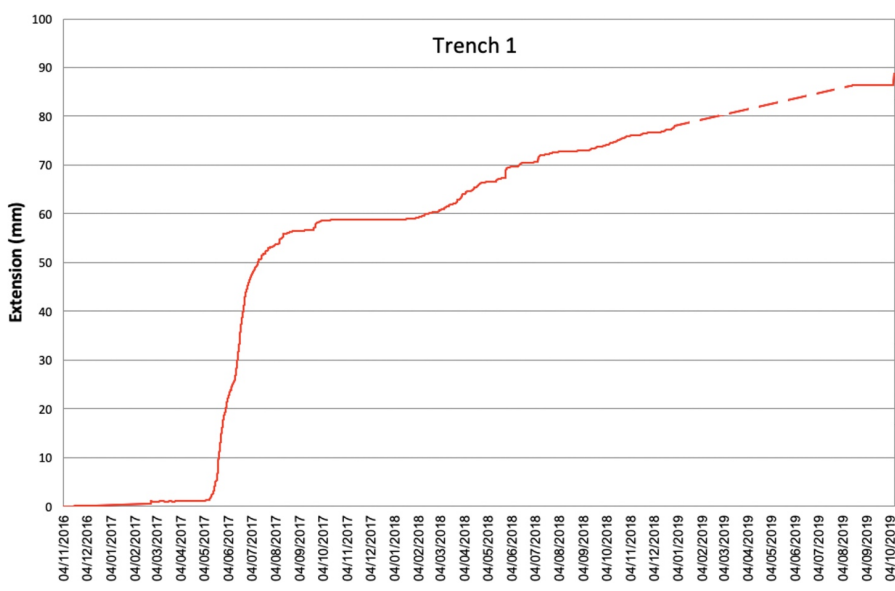
255
 256 **4 Results**
 257 **4.1 Extensometer data**

258 The measurements here described reflect the real extension of this part of the slope, and cannot be
 259 related to the transit of heavy tracks along the road for the following reasons: the two instruments are

260 encapsulated in concrete boxes, and moreover between the instruments and the road asphalt there is
261 a 50-cm-thick layer of reinforced concrete installed during the Soviet period. This clearly protects the
262 extensometers from effects of trucks transit. Moreover, the extensometers recorded long periods of
263 increase and decrease of extension movements, whereas trucks are always present.

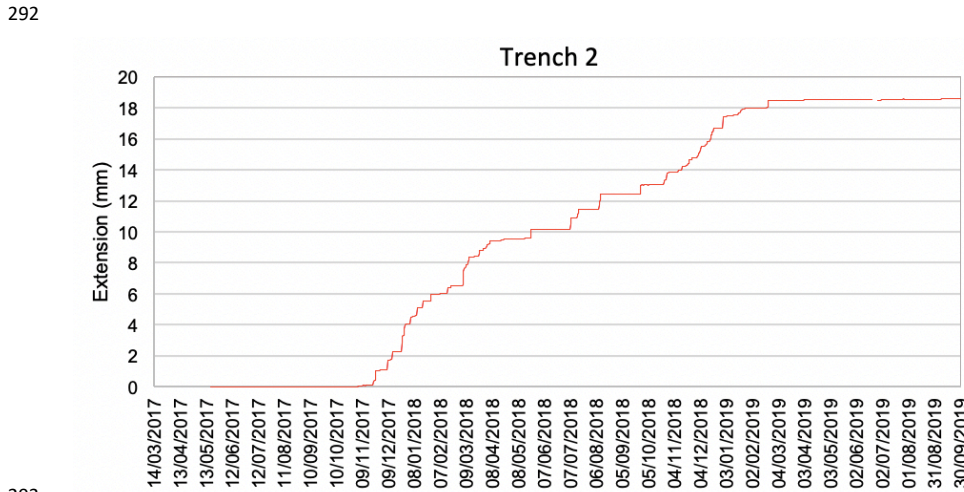
264 Figure 6 shows the readings collected over a 35-month interval, between 4 November 2016 and 9
265 October 2019, by the extensometer at station n. 1. The overall extension recorded during the 35-
266 month period is equal to 88.7 mm, corresponding to an average extension rate of 0.08 mm/day (that
267 is 30.8 mm/y). Extension peaked from 16 May 2017 to 8 August 2017, with a total extension of 52
268 mm, corresponding to an average rate of 0.61 mm/day. This documented acceleration in the
269 movement coincided with the opening of new fractures on the road surface at about 700 m of altitude,
270 i.e. 230 m above the average lake level of 470 m a.s.l.

271 From 3 October 2017, extension ceased until 16 January 2018. This date marks the beginning of
272 another period of slight extension, lasting until 6 March 2018. From this date on, another interval of
273 extension rate increase was recorded, although much less pronounced than the previous one. This
274 increase lasted until 22 May 2018, marked by a rate of 0.12 mm/day. From the end of May 2018 to
275 October 2019, extension was linear with a rate of 0.04 mm/day, with a data gap between
276 30/12/2018 and 13/8/2019 due to a technical problem. This slower, creep-like movement was
277 accompanied by the development of small sinkholes and fractures within the landslide body.



280 **Figure 6.** Graph showing the readings of the incremental extension (in mm), associated with
281 landslide surface displacement, recorded by station n.1 from November 2016 to October 2019.

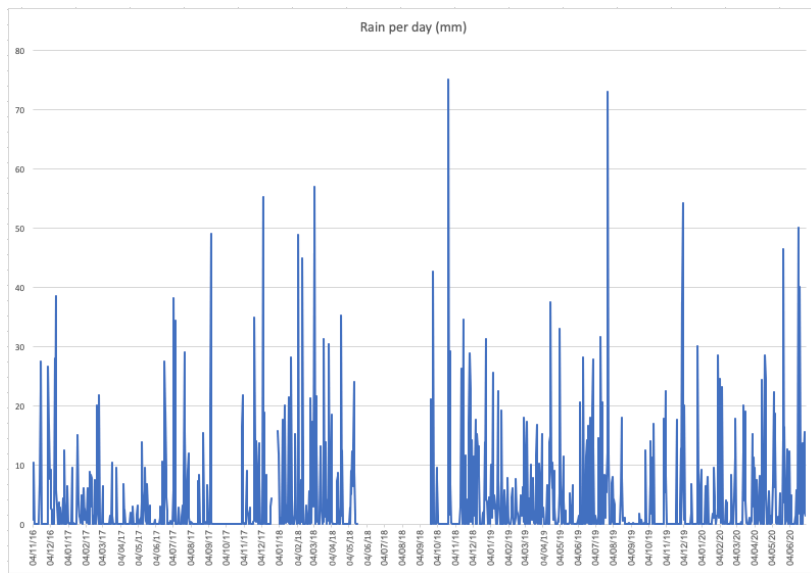
282
283 Regarding extensometer n. 2, data are shown over a 28.5-month interval (from 18 May 2017 to 30
284 September 2019) (Fig. 7). Here, the total amount of extension was 19.14 mm, with an average
285 extension rate of 0.02 mm/day (that is 8.17 mm/y). From the beginning until 24 October 2017, there
286 was a steady slight extension, followed by a period of high deformation expressed, in the graph, by a
287 line with an upward convexity, indicating firstly a strong increase and later on a gradual decrease in
288 the extension rate. This period lasted until 27 February 2018 and was characterized by an average
289 rate of 0.16 mm/day, followed by another increase for one month, and then by a steady extension
290 until 15 November 2018. Thereafter, until 29 January 2019, a new increase in the extension rate was
291 observed, after which extension ceased.



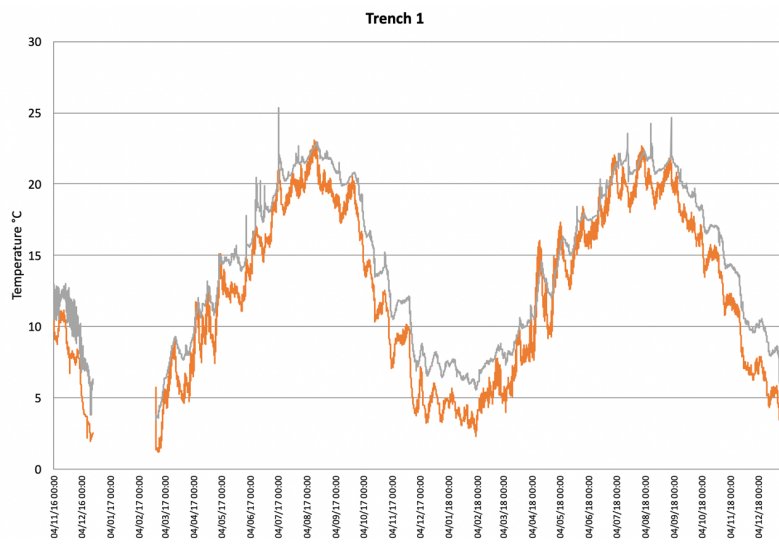
296
297 **4.2 Meteorological data**
298 The amount of rainfall shows important variations (Fig. 8). Rainy days are mostly characterized by
299 amounts within 10-20 mm/day. Peaks of 40-50 mm/day were recorded on 7/9/17, 5/2/18, 12/2/18,
300 26/9/18, 23/5/20 and 18/6/20. Peaks between 51-60 mm/day occurred on 6/12/17, 5/3/18 and 1/12/19.
301 The highest peaks, above 70 mm/day, took place on 22/10/18 and 25/7/19. Periods of particularly

302 heavy rains were recorded from 19/1/18 to 12/5/18 and from 22/9/18 to 16/1/19. From middle April
303 2018 to 25 September 2018, there was a gap in the data due to technical problems.
304 As regards temperatures (T), these show a double fluctuation (Fig. 9); the short-term fluctuation took
305 place within a frequency of 5-20 days, whereas the long-term fluctuation developed each 12 months.
306 At Trench 1, in the first period of observations, the T at the data logger, near the ground surface,
307 gradually decreased to 3° on 22/2/17, though there was a gap in data, due to a technical problem, from
308 mid- December 2017 to mid-February 2017. Then, T increased until it peaked to 22.9° on 15/8/17.
309 From this date until 2/2/18, there was a gradual decrease, until a minimum of 5.5° was reached. Then
310 T increased again and reached a maximum of 22.4° on 10/8/18. T then decreased down to 0.9° on
311 27/12/18. At Trench 2 the variations of T were similar to Trench 1, although the absolute values were
312 sometimes higher, in the order of 1°-2°.
313 The T of the wire inside the instrument recorded the same pattern of variations, although smoothed,
314 with T systematically higher, in the order of 3°-4° at Trench 1, and with a much smaller difference at
315 Trench 2 (Fig. 9). This different pattern can be due to the fact that in Trench 2 there is a greater
316 circulation of water than in the other trench, and thus the temperature tends to be more balanced due
317 to a better thermal conductivity of water than air.

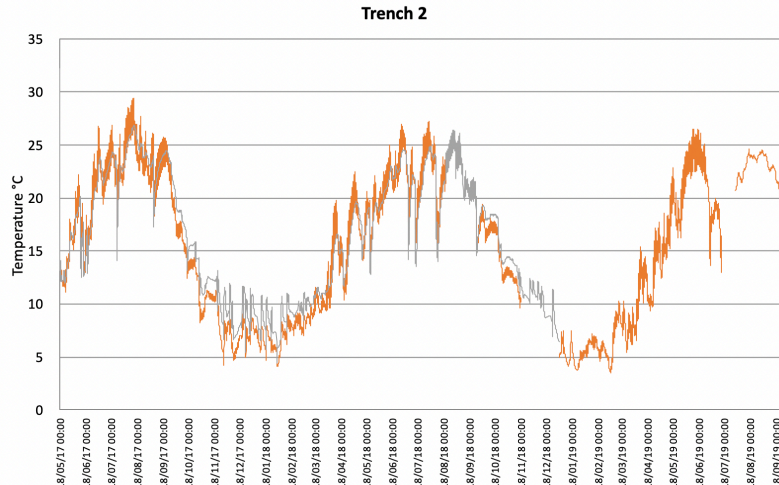
318



319
320 **Figure 8.** Amount of rainfall recorded near the landslide, from 4 November 2016 to 30 June 2020.
321



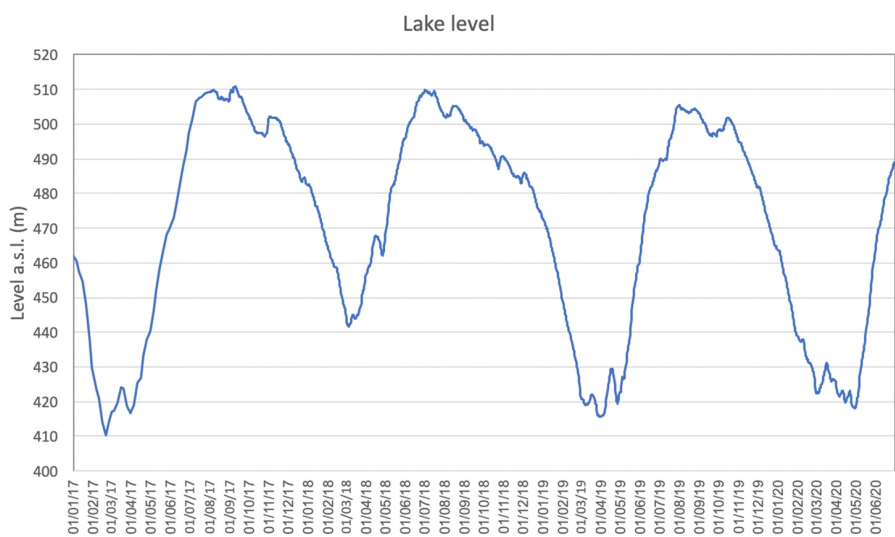
324 **Figure 9.** Temperatures recorded at Trench 1 from November 2016 to December 2018, and at Trench
 325 2 from May 2017 to September 2019. The grey line represents the variations in temperature of the
 326 extensometer wire, inside the instrument, whereas the orange line shows temperature variations at
 327 the data logger that is near the ground surface.



331 **4.3 Lake level data**

332 Since the beginning of our measurements (1 January 2017) until 20 February 2017, there was a
333 continuous emptying of the reservoir, the level of which dropped down to a minimum of 410 m a.s.l.
334 (Fig. 10). Thereafter, the reservoir was filled again, to a maximum of 510 m on 5 August 2017,
335 followed by a further increase on 12 September 2017, up to 511 m. From this date on, there was a
336 decrease of the lake level until 29 February 2018, when it reached an altitude of 443 m. Then, it
337 increased again reaching the altitude of 510 m on 30 June 2018. Later on, a new period of level
338 decrease lasted until 31 March 2019, when lake level reached 414 m. Over the next month there was
339 an oscillation with an increase of 35 m followed by a decrease. From 23 April 2019, a lake level
340 increase was recorded, which ended on 26 July 2019, reaching an altitude of 507 m. Thereafter, a
341 new period of lake level decrease took place, until 29 April 2020 when it reached 419 m.

342



343

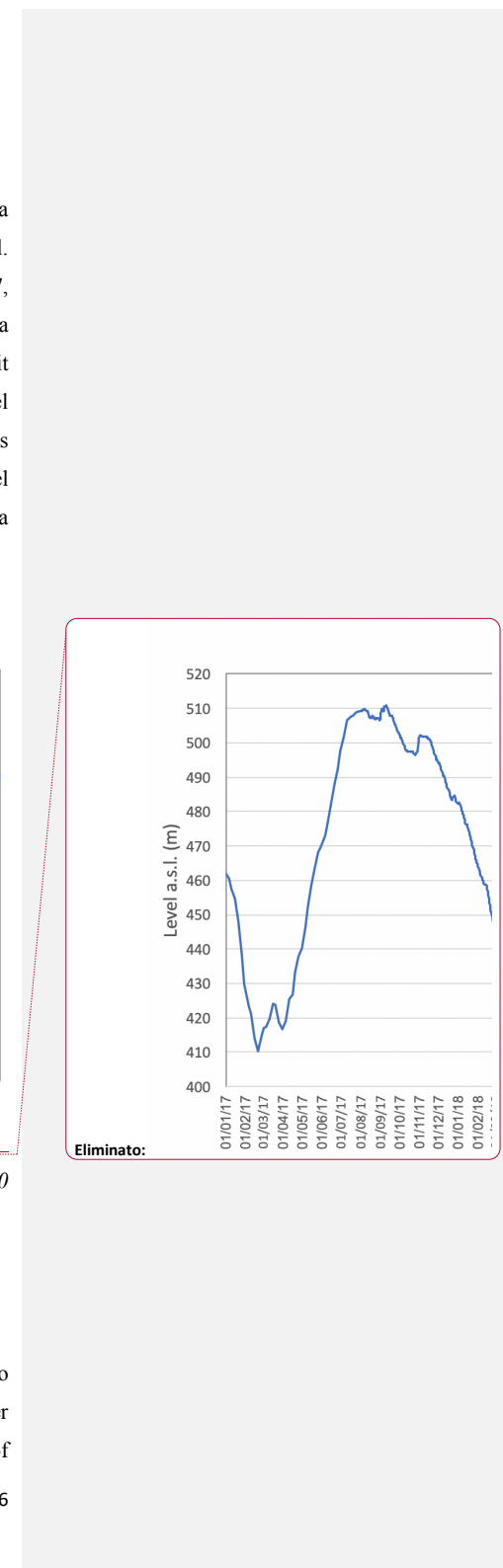
344 **Figure 10.** Variations of the level of the Enguri artificial water reservoir from 1 January 2017 to 30
345 June 2020.

346

347 **5 Discussion**

348 **5.1 Correlation of slope deformation - lake level - rainfall**

349 Here, we briefly discuss all the data, which we have combined in the graphs of Figure 11, so as to
350 provide a more immediate interpretation. In this graph we also report the rainfall cumulated per
351 month, in order to better quantify its possible influence. At extensometer n. 1, the total amount of



353 extension has been 88.7 mm in 35 months, yielding an average extension rate of 0.08 mm/day.
354 Extension peaked from 16 May 2017 to 8 August 2017, with a total extension of 52 mm that
355 corresponds to a rate of 0.61 mm/day, about eight times the average extension rate during the whole
356 measurement period. This extension rate increase follows the almost complete drawdown of the lake
357 (which went down to the lowest level on 21 February 2017) and the ensuing period of lake level
358 infilling, with a 100-m water level increase. A delay of about one month can be recognized between
359 the lake level increase and the extension rate increase, but the shape and duration of the period of
360 extension increase mimics exactly the shape and duration of the lake infilling (segments between
361 arrows in Fig. 11), suggesting a strong correlation. Another interval of extensional rate increase,
362 although much smoother than the previous one, is recognizable during a period after 6 March 2018,
363 at the same time as a 67-m increase of the water level. During the third period of lake filling and
364 refilling, due to technical problems at the extensometer, possible further rate variations were not
365 recorded. During periods of water level lowering, instead, the extension rate tends to decrease to the
366 lowest values.

367 At extensometer 1, there is no correlation between rainfall amounts and extension rate values in the
368 period 11/2016 – 4/2017, during which the extension curve is subhorizontal in spite of rainfall
369 variations. Similarly, there is no correlation between rain and extension when there is the strongest
370 extension increase of 5/2017 – 8/2017, because this follows a period of low rain precipitations. On
371 the contrary, this extension rate increase perfectly matches, after one month, the lake level increase.
372 The other period of extension increase from 2/2018 to 5/2018 coincides with the second lake level
373 increase, but it follows also a period of rainfall intensification (11/2017-2/2018). We suggest that, in
374 this case, cumulated rainfall might have contributed to increasing the extension rate owing to water
375 infiltration into the slope, though this is masked by lake level increase and we do not have data on the
376 variation of water saturation in the landslide slope.

377 At extensometer n. 2, the total amount of extension was 19.14 mm in 28.5 months, with an average
378 extension rate of 0.02 mm/day. There is no correlation between the amount of rainfall and extension
379 rate values in the period 5/2017 – 10/2017, during which the extension curve is subhorizontal in spite
380 of rainfall variations. Extension increased, from 31 October 2017 to 1 April 2018, to 0.13 mm/day,
381 corresponding to a 5-month interval of increased deformation, in a much similar way as at
382 extensometer n. 1, over a three-month period. It is worth noting that the extension curves derived
383 from the two extensometers have a similar shape, but at extensometer n. 2 the curve is shifted onward
384 by four to six months. This period of extension increase coincides with the lake level decrease, but it
385 also coincides with a period of rainfall increase. We suggest that these accelerated movements at
386 extensometer n. 2 may have been triggered by the previous movements within the landslide sector

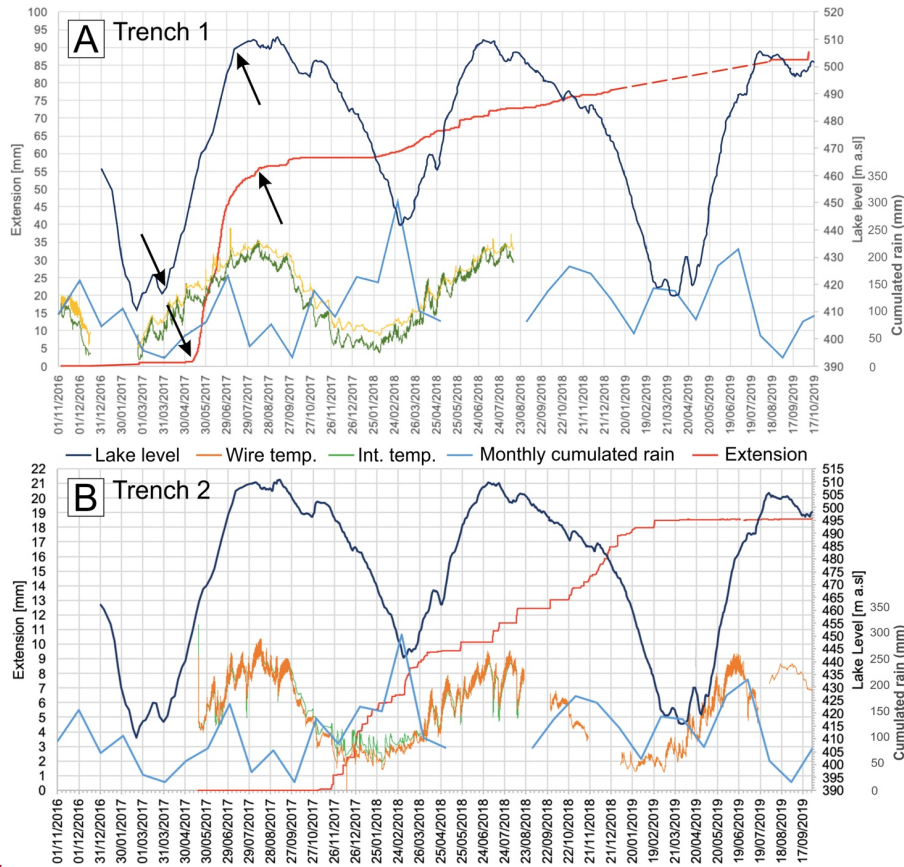
387 where extensometer n. 1 is located, as it will be highlighted in the following chapter, in possible
388 combination with rain infiltration in the slope. At extensometer n. 2, the extension curve is still steep
389 in the following period until 7/2018, which is coincident with a lake level increase, followed by a
390 further extension rate increase until 1/2019, in correspondence of lake level decrease and strong
391 rainfall.

392 As documented by Tibaldi et al. (2019), based on the analysis of the Quaternary geological deposits
393 of the area, and by the presence of the high head scarp, the landslide area had already been subject to
394 slope failure events during prehistoric times. As a consequence of this, the processes that have taken
395 place along and across the slope during lake level variations, have been affecting an already
396 destabilized slope, which is expected to be more sensitive to variations of the conditions at its toe. In
397 general, the presence of artificial lakes can trigger possible seepage process accompanied by an
398 increase in pore water pressure in the slope deposits, with the effect of reducing their shear strength.
399 At the same time, the presence of a water basin may lead to a stabilization of the submerged part of
400 the slope (Paronuzzi et al., 2013). In transient conditions, lake filling or drawdown can trigger
401 landslides (Schuster, 1979; Kenney, 1992; Zhu et al., 2011). In a similar way to the Enguri case, pre-
402 existing, ancient landslides were reactivated during the filling of the water reservoir at the Włocławek
403 dam in Poland (Kaczmarek et al., 2015). This cause-effect relation is even more apparent, where
404 bank-forming materials have a high permeability, like in the study area, in which the slope is mostly
405 made of debris and highly fractured materials; within highly permeable deposits, a reservoir level
406 increase can trigger a rapid reservoir-induced water inflow that reduces both the strength and the
407 factor of safety. This occurred, for example, at the October 1963 Vajont landslide in NE Italy: as
408 documented by Paronuzzi et al. (2013), among the triggering factors for the disaster, a predominant
409 role was played by reservoir level increase, and by the presence of an already existing landslide.
410 Another example comes from the Byford Creek landslide, located above the Clyde artificial reservoir
411 in New Zealand, where lake filling produced a major increase in extension rate, followed by long-
412 term creep movements (Macfarlane, 2009).

413 To summarize the above, our data show that, at least during the first period of extension increase at
414 extensometer n. 1, the slope still has a high sensitivity to water infilling operations more than 40 years
415 after the construction of the Enguri reservoir. The presence of highly-permeable deposits in the lower
416 part of a slope, as is the case at the Khoko landslide, represents a key aspect to be considered for the
417 assessment of hydrogeological hazard. In such a case, during reservoir level increase, the water pore
418 pressure effects on shear strength prevail over the stabilizing and buttressing effects induced by the
419 water body, resulting in an acceleration in slope movements. For the other periods of extension

420 increase, an effect of rainfall intensification cannot be excluded, whereas extensometer n. 2 may also
 421 have reacted to deformation of the slope part where the other extensometer n. 1 is located.

422

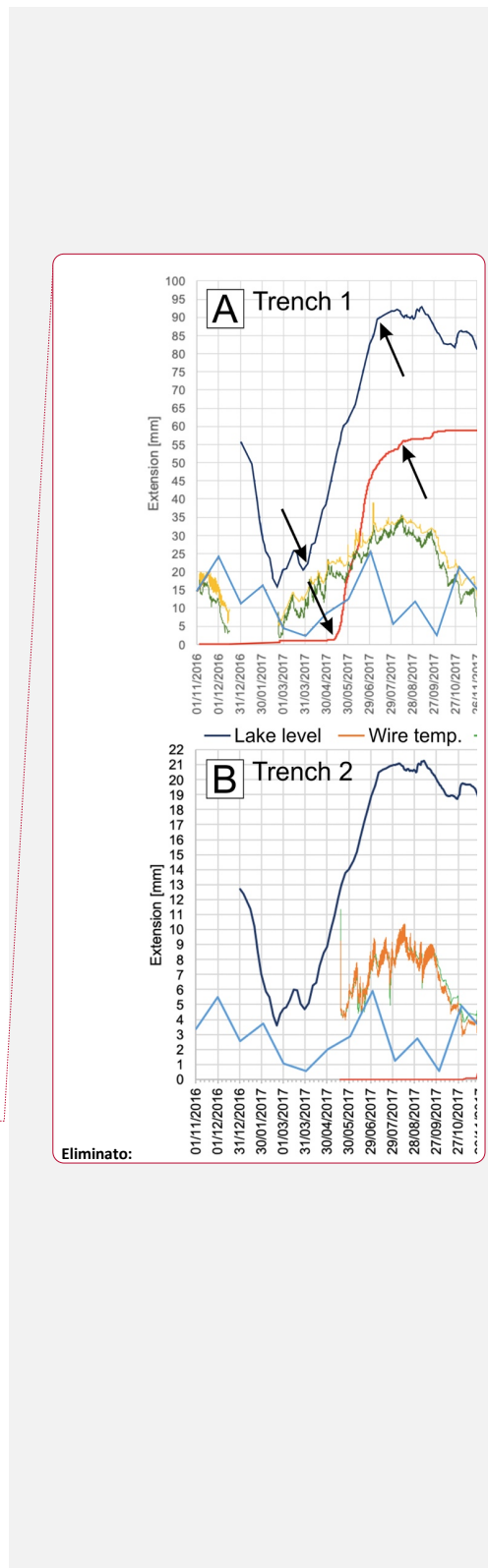


423
 424 **Figure 11.** Graphs showing the combination of all data collected at trench 1 (A) and trench 2 (B).
 425 Note that rainfall is expressed as cumulated month precipitation. The arrows point to the segments
 426 of the extension and lake level curves that show similar shape at short time distance.

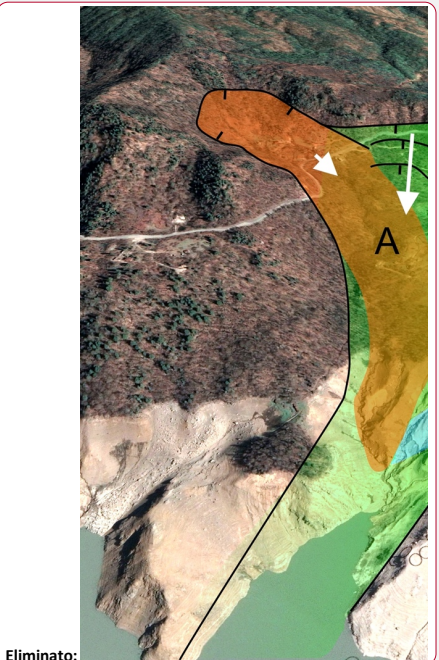
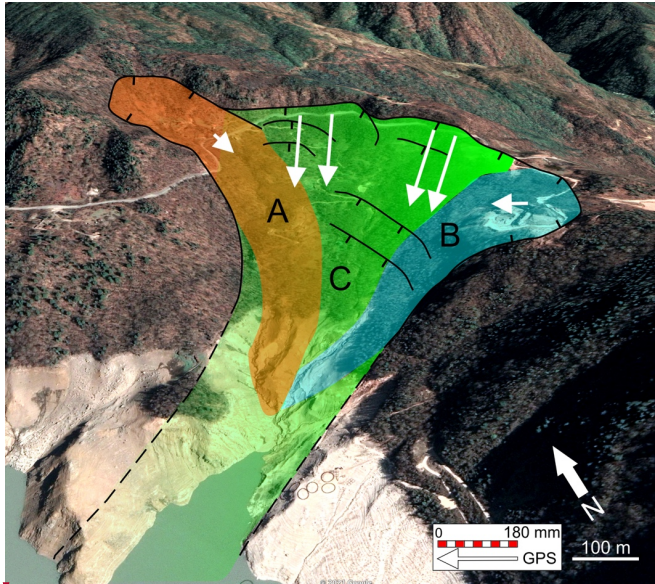
427

428 5.2 Behaviour of the landslide and slip planes

429 The hypothesis introduced in the previous chapter proposes that during the first and greatest lake level
 430 increase, there was an increment in water pore pressure within the slope with a consequent decrease
 431 of the shear strength. This seems to have produced an increase in extension at the two trenches with



433 a time offset. Another possibility is that the lake level increase triggered slope deformation only at
434 the landslide sector where extensometer n. 1 is located, whereas the other landslide portion, where
435 extensometer n. 2 is located, initially remained stable but, later on, deformation was triggered also
436 there. The different patterns observed at the two trenches may be explained in terms of the fact that
437 they are located in two different sectors of the general landslide, which can move separately. The
438 possible presence of different sectors within the general landslide body is suggested by underground
439 data and by GPS data. Based on the results summarized in Figure 4, a number of possible slip planes
440 affect the landslide, from shallow to deeper ones. Moreover, the slip planes modeled through our
441 static analysis are of two types: slip planes that initiate at the head scarp and prolong downward to
442 the valley bottom (now covered by the lake), and slip planes that run from the head scarp to half of
443 the slope, reaching the present lake's coastline. The presence of multiple slip planes at different depths
444 is supported also by the documented ruptures of piezometers at different depths. These slip planes
445 clearly correspond to different portions of the landslide that might move, at least in part,
446 autonomously from each other. GPS stations were installed in the upper part of the landslide and were
447 operational during most of the 2016-2019 observation period (Ospanov and Krivchenko, 2021). Four
448 GPS stations are characterized by motion vectors with the same cumulated magnitude of movement
449 (160-183 mm) and the same orientation (the central four arrows in Fig. 12), whereas the other two
450 GPS stations show different magnitude of movement (48 mm the GPS located west, and 80 mm the
451 GPS located east in Fig. 12) and different, opposite orientations. Based on these data and
452 geomorphological evidence, we suggest the possible presence of three main landslide sectors: two
453 corresponding to shallower landslides (A and B in Fig. 12) and one deeper (C in Fig. 12).
454 On the other hand, during the decrease of the lake level, extension increases at both trenches, as is
455 the case, for instance, at the very beginning of 2018. This increase in extension might be due to the
456 debuttressing of the slope toe associated with the emptying of the lake, resulting in a more widespread
457 mobilization of the landslide and probable inception of slip along the deeper planes. As already
458 suggested in the previous chapter, we cannot rule out the possibility that water infiltration due to
459 periods of increased rainfall might also have contributed to increasing the extension rate.
460



461
462 **Figure 12.** Sketch of the possible different units that compose the general landslide onshore. The
463 green unit C corresponds to a deeper-seated slope deformation, whereas the orange (A) and the blue
464 (B) units are shallower bodies. White arrows represent GPS vectors collected by Ospanov and
465 Krivchenko (2021). Black lines are the main scarps affecting the slope.

466
467 **6 Data availability**
468 The databases showcased in this work are available for download from the UniData Repository
469 (Milan, Italy) at <https://www.unidata.unimib.it/?indagine=deformation-and-meteorological-data-of-the-khoko-landslide-enguri-republic-of-georgia-2016-2020>, DOI: 10.20366/unimib/unidata/SI384-
470 1.1 (Tibaldi et al., 2020). The extension dataset is provided in two separate files, for Trench 1 and for
471 Trench 2, in tab format (extension data with frequency sampling of 60 min) together with air
472 temperature near the ground surface (frequency sampling of 60 min), and temperature of the
473 extensometer wire in the interior of the instrument (frequency sampling of 60 min). At the same web
474 link is available the file of meteorological data (frequency sampling of 1 day) and lake level variations
475 (frequency sampling each 5 days until 30/7/17 and then each one day).

476
477
478 **7 Conclusions**
479 At the major Khoko landslide, located on the eastern side of the Enguri artificial water reservoir, a 4-
480 year-long campaign of measurement, by way of two digital extensometers, enables documenting the

482 activity of the mass movement, at a rate of 8.2 mm/yr to 30.8 mm/yr depending on the site of
483 measurement. During this period, we observed a correlation between the greatest, rapid infilling of
484 the lake and an increase in deformation rate of the slope. Deformation of the landslide at extensometer
485 n. 1, thus, appears to have been controlled by variations in hydraulic load, induced mainly by lake
486 oscillations. There is a systematic delay between man-induced lake oscillation and the response of
487 the landslide mass, quantifiable in about one month at extensometer n. 1. Increase of extension at
488 extensometer n. 2 may, in turn, have been triggered by the previous deformation that occurred in the
489 landslide sector where the other extensometer is located. These results, together with the different
490 slip rates at the two instruments, the presence of different slip planes at various depths, and the
491 different orientations and amounts of movement measured at GPS stations located in the landslide,
492 suggest that the Khoko landslide is composed of more than one unstable block, each of which can
493 behave in a different way. Moreover, a possible correlation with heavier rainfall has been observed
494 for some periods of increased extension, and thus we cannot rule out the possible contribution of
495 water infiltration in the slope. This overall monitoring effort will help individuate possible future
496 accelerations of deformation at the unstable mass overlooking the Enguri artificial reservoir.

497
498 **Author contributions.** AT coordinated the research and wrote most of the paper. PO designed and
499 maintained the sensor network. FPM and FB contributed to the geological and geomorphological
500 mapping of the landslide area. NT coordinated and contributed to collecting extension data at the
501 extensometers. LM and JC provided meteorological and lake level data.

502
503 **Competing interests.** The authors declare they have no conflict of interest.

504
505 **Acknowledgements.** We are indebted to the Ministry of Infrastructure of Georgia that helped us to
506 obtain the permission to work along the Jvari-Khaishi-Mestia road. We also wish to thank four
507 anonymous reviewers for their precious and helpful comments and suggestions.

508
509 **Financial support.** This research was conducted with the financial help from NATO project SfP
510 G4934 "Georgia Hydropower Security", the International Lithosphere Program - Task Force II, and
511 project 216758 of the Shota Rustaveli National Science Foundation. Satellite images were provided
512 in the framework of the European Space Agency project n. 32309 "Active tectonics and seismic
513 hazard of southwest Caucasus by remotely-sensed and seismological data".

514
515 **References**

516 Bertolini, G., Guida, M., & Pizzoli, M. (2005). Landslides in Emilia-Romagna region (Italy):
517 strategies for hazard assessment and risk management. *Landslides*, 2(4), 302-312.
518 Bitelli, G., Dubbini, M., & Zanuttta, A. (2004). Terrestrial laser scanning and digital photogrammetry
519 techniques to monitor landslide bodies. *International Archives of Photogrammetry, Remote Sensing*
520 and Spatial Information Sciences, 35(B5), 246-251.
521 Casagli, N., Tibaldi, A., Merri, A., Del Ventisette, C., Apuani, T., Guerri, L., Fortuny-Guasch J. &
522 Tarchi, D. (2009). Deformation of Stromboli Volcano (Italy) during the 2007 eruption revealed by

523 radar interferometry, numerical modelling and structural geological field data. *Journal of*
524 *Volcanology and Geothermal Research*, 182(3-4), 182-200.

525 Fell, R., Ho, K. K., Lacasse, S., & Leroi, E. (2005). A framework for landslide risk assessment and
526 management. *Landslide risk management*, 3-25.

527 Froude, M. J. and Petley, D. N., 2018. Global fatal landslide occurrence from 2004 to 2016, *Nat.*
528 *Hazards Earth Syst. Sci.*, 18(8), 2161–2181, doi:10.5194/nhess-18-2161-2018.

529 Gulen L., and EMME WP2 Team (2011). Active faults and seismic sources of the Middle East region:
530 earthquake model of the Middle East (EMME) project. In: *Abstracts of the AGU Fall Meeting*, San
531 Francisco, California, 5-9 December 2011.

532 Kaczmarek, H., Tyszkowski, S., and Banach, M., 2015. Landslide development at the shores of a
533 dam reservoir (Włocławek, Poland), based on 40 years of research, *Environmental Earth Sciences*,
534 74(5), 4247-4259.

535 Kenney, T.C., 1992. Slope stability in artificial reservoirs: influence of reservoir level, selected cases,
536 and possible solutions, In: Semenza, E., Melidoro, G. (Eds.), *Proceedings of the meeting on the 1963*
537 *Vajont landslide*, 17-19 September 1986, Ferrara, Cansiglio and Vajont. Grafica Ferrarese, Ferrara,
538 Italy, 67-85.

539 Koçyigit, A., Yılmaz, A., Adamia, S., and Kuloshvili, S. (2001). Neotectonics of East Anatolia
540 Plateau (Turkey) and Lesser Caucasus: Implication for transition from thrusting to strike-slip faulting.
541 *Geodin. Acta*, 14, 177-195.

542 Liu Shao-tang 2006. Deformation measurements during the construction of large dam projects.
543 *Chinese Journal of Underground Space and Engineering* 06(Z2): 1346–1348.

544 Liu, S. T., and Wang, Z. W. (2008). Choice of surveying methods for landslides monitoring. In
545 *Landslides and engineered slopes: from the past to the future. Proceedings of the tenth international*
546 *symposium on landslides and engineered slopes*. Taylor & Francis, Xi'an.

547 Macfarlane, D.F., 2009. Observations and predictions of the behaviour of large, slow-moving
548 landslides in schist, Clyde Dam reservoir, New Zealand, *Engineering Geology*, 109(1-2), 5-15.

549 Ospanov N. S., and Krivchenko, A. A., 2021. Description of a 2-Year, High-Resolution Geodetic
550 Monitoring of the Khoko Landslide, Enguri Reservoir, Georgia. In: F. L. Bonali et al. (eds.), *Building*
551 *Knowledge for Geohazard Assessment and Management in the Caucasus and other Orogenic*
552 *Regions*, NATO Science for Peace and Security Series C: Environmental Security, Springer Nature,
553 301-316, doi.org/10.1007/978-94-024-2046-3_16.

554 Paronuzzi, P., Rigo, E., and Bolla, A., 2013. Influence of filling–drawdown cycles of the Vajont
555 reservoir on Mt. Toc slope stability, *Geomorphology*, 191, 75-93.

556 Pasquaré Mariotto F., Tibaldi A. (2016). Inversion kinematics at deep-seated gravity slope
557 deformations revealed by trenching techniques. *Nat. Hazards Earth Syst. Sci.*, 16, 663-674.

558 Pasquaré, F., Tormey, D., Vezzoli, L., Okrostsvardze, A., Tutberidze, B. (2011). Mitigating the
559 consequences of extreme events on strategic facilities: Evaluation of volcanic and seismic risk
560 affecting the Caspian oil and gas pipelines in the Republic of Georgia. *J. Environ. Man.*, 92, 1774–
561 1782.

562 Reilinger, R. E., McClusky, S. C., Oral, M. B., King, R. W., Toksoz, M. N., Barka, A. A., Kinik, I.,
563 Lenk, O., and Sanli, I. (1997). Global Positioning System measurements of present-day crustal
564 movements in the Arabia-Africa-Eurasia plate collision zone. *J. Geophys. Res.*, 102, 9983–9999.

565 Reilinger, R. E., McClusky, S. C., Vernant, P., Lawrence, S., Ergintav, S., Cakmak, R., Ozener, H.,
566 Kadirov, F., Guliev, I., Stepanian, R., Nadariya, M., Hahubia, G., Mahmoud, S., Sakr, K., Arrajehi,
567 A., Paradissis, D., Al-Aydrus, A., Prilepin, M., Guseva, T., Evren, E., Dmirotsa, A., Filikov, S. V.,

568 Gomez, F., Al-Ghazzi, R., Karam, G. (2006). GPS constraints on continental deformation in the
569 Africa-Arabia-Eurasia continental collision zone and implications for the dynamics of plate
570 interactions. *J. Geophys. Res.*, 111, B05411, <https://doi.org/10.1029/2005JB004051>.

571 Schuster, R.L., 1979. Reservoir-induced landslides, *Bulletin of the International Association of*
572 *Engineering Geology*, 20, 8-15.

573 Spiker, E. C., & Gori, P. (2003). National landslide hazards mitigation strategy, a framework for loss
574 reduction (No. 1244). US Geological Survey.

575 Tibaldi, A., Pasquaré F. (2008). Quaternary deformations along the “Engadine–Gruf tectonic
576 system”, Swiss–Italian border. *J. Quaternary Sci.*, 23 475–487.

577 Tibaldi, A., Rovida, A., Corazzato C. (2004). A giant deep-seated slope deformation in the Italian
578 Alps studied by paleoseismological and morphometric techniques. *Geomorphology*, 58, 27–47.

579 Tibaldi, A., Corazzato, C., Rust, D., Bonali, F. L., Pasquaré Mariotto, F., Korzhenkov, A. M., Oppizzi
580 P., and Bonzanigo, L. (2015). Tectonic and gravity-induced deformation along the active Talas–
581 Fergana Fault, Tien Shan, Kyrgyzstan. *Tectonophysics*, 657, 38–62.

582 Tibaldi, A., Alania, V., Bonali, F. L., Enukidze, O., Tsereteli, N., Kvavadze, N., Varazanashvili, O.
583 (2017a). Active inversion tectonics, simple shear folding and back-thrusting at Rioni Basin, Georgia.
584 *J. Struct. Geol.*, 96, 35–53.

585 Tibaldi, A., Russo, E., Bonali, F. L., Alania, V., Chabukiani, A., Enukidze, O., Tsereteli, N. (2017b).
586 3-D anatomy of an active fault propagation fold: a multidisciplinary case study from Tsaishi
587 (Georgia), western Caucasus. *Tectonophysics*, 717, 253–269.

588 Tibaldi, A., Korzhenkov, A.M., Pasquaré Mariotto, F., Rust, D., Tsereteli, N. (2018). NATO and
589 earth scientists: An ongoing collaboration to assess geohazards and contribute to societal security in
590 Central Asia and the Caucasus. *Episodes*, 41, 193–205.

591 Tibaldi, A., Oppizzi, P., Gierke, J. S., Oommen, T., Tsereteli, N., Gogoladze, Z. (2019). Landslides
592 near Enguri dam (Caucasus, Georgia) and possible seismotectonic effects. *Natural Hazards and Earth*
593 *System Sciences*, 19, 71.

594 Tibaldi, A., Oppizzi, P., Bonali, F., Pasquarè Mariotto, F., Tsereteli, N., Mebonia, L., 2020.
595 Deformation and meteorological data of the Khoko landslide, Enguri, Republic of Georgia. UniData
596 - Bicocca Data Archive, Milan. Study Number SI384, Data file version 1.0 DOI:
597 10.20366/unimib/unidata/SI384-1.1

598 Tsereteli, N., Tibaldi, A., Alania, V., Gventsadse, A., Enukidze, O., Varazanashvili, O., Müller B. I.
599 R. (2016). Active tectonics of central-western Caucasus, Georgia. *Tectonophysics*, 691, 328–344.

600 Varazanashvili, O., Tsereteli, N., Bonali, F. L., Arabidze, V., Russo, E., Pasquaré Mariotto, F.,
601 Gogoladze, Z., Tibaldi, A., Kvavadze, N., Oppizzi, P. (2018). GeoInt: the first macroseismic intensity
602 database for the Republic of Georgia. *J. Seismol.*, 1–43, <https://doi.org/10.1007/s10950-017-9726-5>.

603 Zhu, D., Yan, E., Hu, G., and Lin, Y. 2011. Revival deformation mechanism of Hefeng Landslide in
604 the Three Gorges Reservoir based on FLAC3D software, *Procedia Engineering*, 15, 2847–2851.